Total column density variations of NO_2 and O_3 by automatic visible spectrometry over Pune, India

G. S. Meena*, D. B. Jadhav and C. S. Bhosale

Indian Institute of Tropical Meteorology, Dr Homi Bhabha Road, Pashan, Pune 411 008, India

A single scattering radiative transfer model has been developed to calculate the air mass factors (AMFs) of NO_2 and O_3 for scattered light observations. The direct and scattered intensities reaching the ground have been calculated using this model, which are utilized for computation of AMFs of these species. AMFs have been used to derive the total column densities (TCDs) from slant column densities (SCDs). Daily intensity data obtained by spectroscopic observations made at Pune (18°32′N, 73°51′E) during May 2000–May 2001 are used for the computation of SCDs of NO_2 and O_3 by differential optical absorption spectroscopy (DOAS) technique. NO_2, O_3, H_2O and O_4 have characteristic absorption features in the visible range 462–498 nm. These features have been used in the DOAS technique. The percentage differential optical depths (DODs) of NO_2, O_3, H_2O and O_4 have been computed. The TCD of O_3 has also been derived by other methods. They are in good agreement with Dobson spectrophotometer observations. Here, the daily and seasonal variations in TCDs of NO_2 and O_3 at Pune for the above period are discussed.

BEGINNING with the pioneering work of Brewer *et al.*[1] and Noxon[2], observations of scattered visible light from the zenith sky have been used to obtain the slant column density (SCD) of stratospheric NO_2. Twilight geometry enhances the path of the sunlight in the stratosphere, allowing more sensitivity to stratospheric absorbers. SCDs of trace constituents are deduced from the spectra by differential absorption spectroscopy. The instrument used here is an automatic spectrometer operated in spectral band 462–498 nm with resolution (1.3 nm) and photomultiplier tube (PMT) as detector. The spectrometer is set to measure intensity absorptions of O_3 and NO_2 twice a day during twilight. Spectra are recorded every 2 min during twilight up to 92° solar zenith angle (SZA). These spectra are analysed by differential optical absorption spectroscopy (DOAS) relative to a reference spectrum taken at low SZA. It is possible to retrieve a large number of trace species simultaneously in UV-visible region using DOAS technique[3–7]. Daily/seasonal variations in total column density (TCD) of NO_2 and O_3 have been studied using spectroscopic observations by several workers[5,6,8–13].

*For correspondence. (e-mail: gsm@tropmet.res.in)

The air mass factor (AMF) of the absorbing species is defined as the ratio of the SCD of the absorber to its vertical column density. Calculations of AMFs have been made using single scattering radiative transfer model[14,15]. This approach assumes that each photon entering the detector is scattered only once before it enters the detector from the zenith direction. The attenuation due to absorption and scattering is calculated along paths through the modelled twilight spherical shell atmosphere for each altitude interval, and the intensity-weighted average path through an absorber having a particular altitude profile is subsequently computed.

A visible spectrometer, which observes the zenith sky, provides the simplest method for routine calculation of the SCDs of NO_2, O_3, H_2O and O_4. Observations of the sunlight scattered from the zenith sky, can be made in any weather. We use mercury spectra and Fraunhofer lines in the reference spectrum for wavelength calibration. Atmospheric gases absorb radiation at characteristic wavelength. The efficiency with which a given gas absorbs radiation is expressed by the absorption cross-section, which is a function of wavelength. The absorption cross-sections of NO_2, O_3, H_2O and O_4 are shown in Figure 1. At wavelengths where the absorption cross-section is small, we can expect solar radiation to reach the ground with little attenuation, while at wavelengths where the absorption cross-section is large, absorption occurs fairly high in the atmosphere. The wavelength ranges were chosen to minimize the spectral overlap between different absorbers, in particular, to avoid spectral interference with the H_2O absorption at 448 nm (ref. 16). Differential rather than absolute cross-sections are used in the analysis procedure. The differential cross-sections represent the departures of the cross sections from a mean of zero over the spectral interval of interest[17]. The intensity observations taken during morning and evening hours for 75–92° SZA are used to find the abundance of NO_2, O_3, H_2O and O_4 using Lambert–Beer's law. SCDs are obtained by matrix inversion technique. Details of the observational technique, method of analysis and computational procedure adopted for retrieving TCD of NO_2 and O_3 are discussed. Comparison of TCDs of O_3 has been made with those obtained by different methods and daily morning/evening variation in NO_2 and O_3 are discussed. Seasonal variation of these species is studied during the year 2000–01.

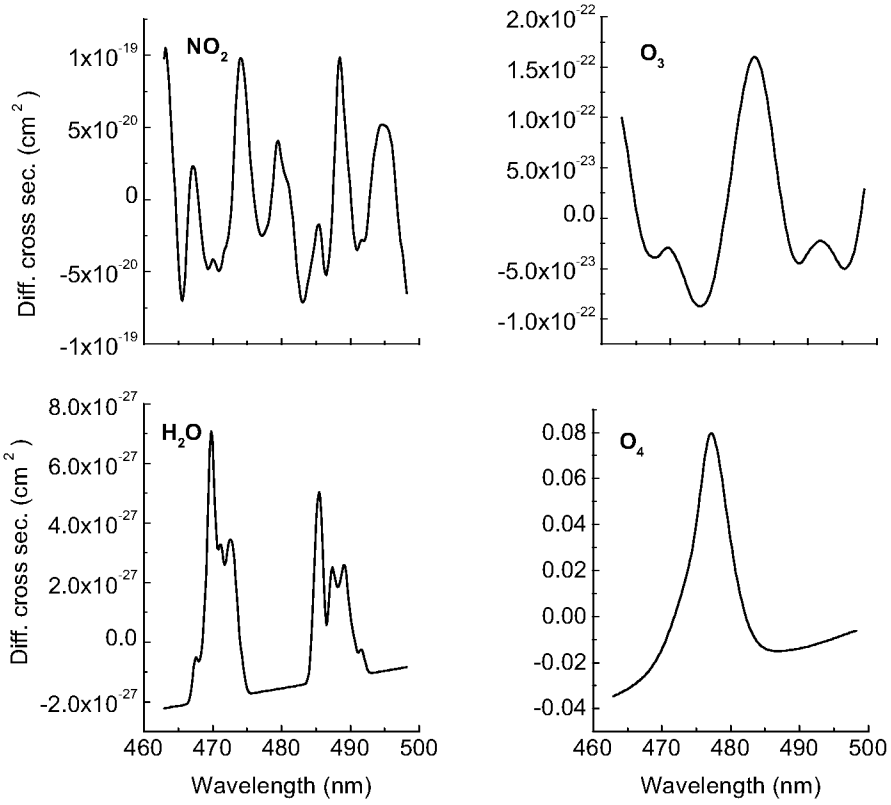

Figure 1. Absorption cross-sections of NO_2, O_3, H_2O and O_4 in the spectral region 462–498 nm.

Methodology

Computations of AMF

The vertical and slant column densities of an atmospheric chemical species are related by

$$S = \delta * V, \tag{1}$$

where S is the slant column density (determined from scattered light absorption measurements) of an absorbing species, V is the vertical column density or TCD of the absorbing species, and δ is the AMF or enhancement in optical path through the absorbing layer.

The optical path enhancement for an atmosphere containing an absorbing layer may be obtained by the Lambert–Beer's law:

$$I = I_0 \exp(-\sigma v \delta), \tag{2}$$

where I and I_0 are the attenuated and incident intensities received by the detector with and without the presence of the absorber, respectively, σ is the cross-section for extinction due to such processes as absorption and scattering by molecules, v is the density of the absorber or scatter. The intensities in eq. (2) are calculated using a radiative transfer model, wherein a particular absorber is introduced to calculate I, and removed to calculate I_0. If the intensity, absorption cross-section and absorber number density are known, then eq. (2) may be inverted for the average enhancement in optical path length or AMF:

$$\delta = -\ln(I/I_0)/\sigma v. \tag{3}$$

Absorption by O_3 and NO_2 is considered in the radiative transfer models used here, together with Rayleigh scattering and atmospheric number density (air density). O_3 and NO_2 profiles are assumed to follow Gaussian distribution. The model spherical shell atmosphere is divided into 50 spherical shells of 1 km thickness for the calculation of AMF. The relevant geometry is depicted in Figure 2. Let us consider the case of single scattering. The contribution to the intensity of scattered radiation by an infinitesimally thin layer at altitude z is given by,

$$I_{sc,z} = I_{d(z)} \sigma_R \, v_{air}(z) \Delta x, \tag{4}$$

where $I_{sc,z}$ is the intensity of scattered radiation at layer z, $I_{d(z)}$ is the intensity of direct flux at altitude z, $v_{air}(z)$ is the atmospheric number density (air density) at altitude z from *Handbook of Geophysics*[18], σ_R is the cross-section for Rayleigh scattering and Δx is the distance over which absorption takes place or the optical path. Proper calculation of Δx is critical, not only due to the absorption of

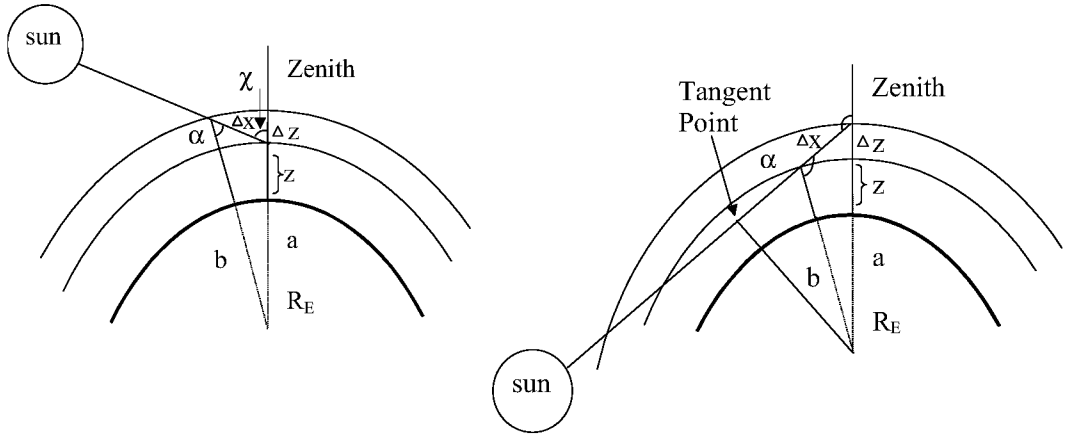

Figure 2. Twilight geometry for direct and scattered radiation and path lengths. ***a***, For $\chi \le 90°$, $a = R_E + z$, $b = R_E + z + \Delta z$, $\alpha = \sin^{-1}[\frac{a}{b}\sin\chi]$, $\Delta X = [a^2 + b^2 - 2ab\cos(\chi - \alpha)]^{0.5}$; ***b***, For $\chi \ge 90°$, $a = R_E + z + \Delta z$, $b = R_E + z$, $\alpha = \sin^{-1}[\frac{a}{b}\sin\chi]$, $\beta = \chi - (180 - \alpha)$, $\Delta X = [a^2 + b^2 - 2ab\cos\beta]^{0.5}$.

radiation by NO_2 and O_3, but also due to the evaluation of the attenuation of incoming solar flux. If the atmosphere is optically thin at the wavelength considered, then all factors except $v_{air}(z)$ in eq. (4) are independent of height, and it follows that the scattered flux varies with altitude as the air density (i.e. exponentially decreasing with increasing altitude). Under these circumstances, most of the singly-scattered photons measured by an upward-looking spectrometer would have been scattered in the lowest few kilometres of the atmosphere. However, for photons at large SZA (greater than about 85°), the atmosphere is far from being optically thin. This is due to the attenuation of solar radiation by Rayleigh scattering, NO_2 and O_3 absorption, so that the direct flux reaching at a particular altitude is reduced according to

$$I_{d(z)} = I_0 \exp[-(\sigma_R \int v_{air}(z) + \sigma_{no2} \int v_{no2}(z) + \sigma_{o3} \int v_{o3}(z))\Delta x]. \quad (5)$$

In eq. (5) I_0, the flux at the top of the atmosphere is considered as 1. The integration of air, NO_2 and O_3 density profiles are taken from altitude z to 50 km. σ_{no2} and σ_{o3} are NO_2 and O_3 absorption cross-sections. $v_{no2}(z)$ and $v_{o3}(z)$ are NO_2 and O_3 density profiles. The maxima of NO_2 and O_3 density profiles are assumed at 15, 20, 25 and 30 km altitude separately. As such, the intensity varies according to the atmospheric density profile, NO_2 absorption, O_3 absorption and strongly with wavelength, since the Rayleigh scattering cross-section varies as the inverse of the wavelength to the fourth power, i.e. $(1/\lambda^4)$. Combining eqs (4) and (5), we obtain the intensity of scattered radiation for any assumed infinitely thin layer:

$$I_{sc,z} = \sigma_R v_{air}(z) I_0 \exp[-(\sigma_R \int v_{air}(z) + \sigma_{no2} \int v_{no2}(z) + \sigma_{o3} \int v_{o3}(z))\Delta x]. \quad (6)$$

Here, the direct and scattered intensities are calculated up to the ground. The direct and scattered fluxes are calculated with and without O_3 absorption by using eqs (5) and (6), and AMFs are obtained using eq. (3). The same procedure is applied for calculations of NO_2 AMFs. The change in atmospheric densities with height has nonlinear effects on the scattered flux and there will be some height z at which maximum scattered intensity occurs. At large SZA, increases in the optical path inhibit the propagation of solar radiation to low altitude, but the radiation that does arrive there will be more strongly scattered. Thus, there will be some altitude z from which most of the radiation reaching the surface is scattered and this will depend upon the path length Δx (which depends upon SZA) and air density profile.

Figure 3 *a* shows the calculated incoming direct flux as a function of altitude for 479 nm wavelength (middle wavelength of the spectral range 462–498 nm) radiations and for various SZAs. Note that there is strong attenuation at low altitude and high SZA. Direct flux at 92, 93 and 94° SZA reaches the altitude at 4, 9 and 16 km, respectively. Figure 3 *b* presents the calculated scattered flux that reaches the surface as a function of the height at which scattering occurs. An upward-looking spectrometer receives light which is a composite of fluxes scattered at all heights, but it is clear from Figure 3 *b* that certain altitudes provide the dominant source of sky brightness at any particular SZA.

Measurements and data

The measurement technique, which is called differential optical absorption spectroscopy, is used for highly structured NO_2 and O_3 absorptions in 462–498 nm range. At twilight, the observed scattered sunlight passes through a long slant path, which enhances the absorptions. The observations are carried out from 75° to 92° SZA. The reference spectra at 38.4° SZA and the observed spectra at 90° SZA (Figure 4) are used to derive the percentage dif-

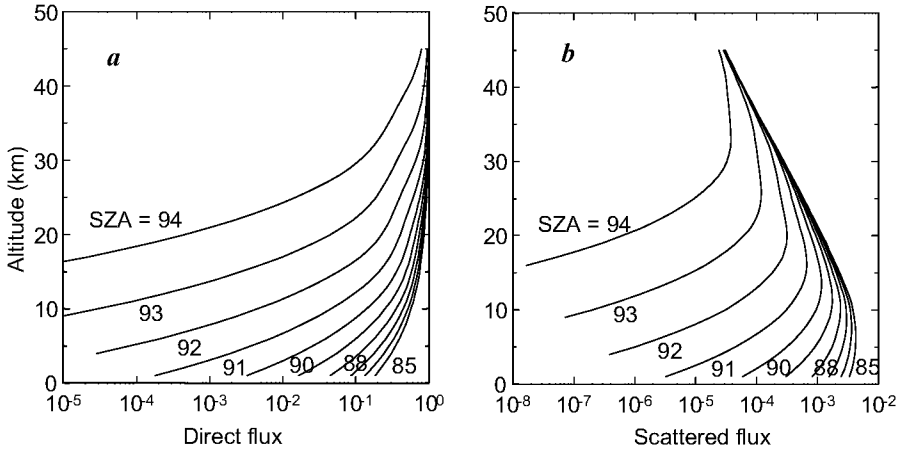

Figure 3. *a*, Calculated intensity of direct flux of solar radiation as a function of altitude for various SZAs; *b*, Scattered flux received from each altitude using zenith-looking spectrometer located at the ground.

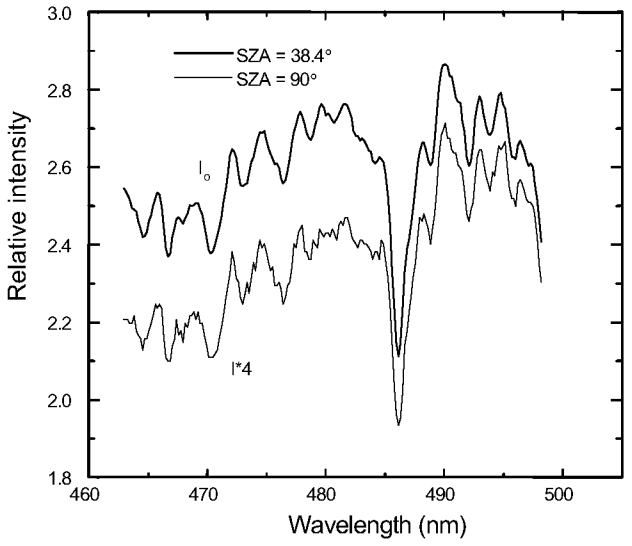

Figure 4. Observed zenith sky absorption spectra.

ferential optical depth (DOD). The observation schedule of the spectrometer programmed for zenith angle setting, interval for observations, signal level expected, latitude/longitude of stations, integration time and number of output samples to be collected is fixed before the observation. Once the observation schedule is set, the spectrometer will automatically take observations. The experimental arrangement and details about the spectrometer are described by Jadhav *et al.*[19] and Meena *et al.*[20].

Observations of the zenith sky light were carried out in the spectral region 462–498 nm during morning and evening twilight periods. The ratio of zenith sky spectra of noontime and evening time is taken to eliminate the Fraunhofer line structure and this ratio spectrum gives the effect of absorption of NO_2, O_3, H_2O and O_4 column relative to the reference spectra, which is used to determine the SCDs of NO_2 and O_3.

Computation of TCD

During the last two decades, the DOAS technique has been developed into a powerful tool for the detection of a variety of atmospheric trace species such as O_3, NO_2, NO_3, OClO, BrO[2,8,15,21,22]. For retrieval of SCDs of trace gases, the spectrum of zenith-scattered light is usually analysed. If the intensities, absorption cross-sections and AMFs are known, then eq. (2) may be inverted for the density of an absorber. The absorber concentration V is derived from eq. (1).

In atmospheric measurements, I_0 cannot usually be determined easily and in addition, the detected light is not only attenuated by the absorption of different atmospheric trace gases, but also by atmospheric Mie and Rayleigh scattering. However, to study NO_2, O_3, H_2O and O_4 by DOAS technique, the ring cross-sections have been considered. Absorption by O_3, NO_2, H_2O and O_4 are derived by matrix inversion technique[15].

Vertical column ozone V is obtained from slant column S, by using the following relationship:

$$V = \frac{S + R}{\mathrm{AMF}}, \tag{7}$$

where R is the slant column amount of absorber in the reference spectrum. The procedure of averaging the density values at twilight hours over a suitable range of SZAS is used here to minimize the errors in the retrieval of vertical column ozone[23,24].

$$\overline{V} = \frac{1}{N} \sum_{\mathrm{SZA}=75}^{90} \frac{S_{\mathrm{SZA}} + R}{AMF_{\mathrm{SZA}}}, \tag{8}$$

where N is the number of spectra measured between 75 and 90° SZA.

Langley plots

Equation (7) may be rearranged as below:

$$S = V \times \mathrm{AMF} - R. \quad (9)$$

The plot of S as a function of AMF for a half-day period, commonly called a Langley plot, should therefore be a straight line.

The line will only be straight if: (i) The AMF calculated is correct; (ii) V does not change during the period; and (iii) the ozone is horizontally uniform. If these conditions are satisfied, the slope of Langley plots (V_{LP}) should give V directly, while the intercept (R_{LP}) corresponds to slant column amount in the reference spectra. Least square straight-line fits, weighted by the inverse square of their standard error, are used to determine R_{LP} and V_{LP} by means of standard formula. The slant column amount of ozone in the noon reference spectrum is calculated from the Dobson spectrophotometer observations also.

$$R_{Dob} = V_{Dob} \times \mathrm{AMF}_{Ref}. \quad (10)$$

Average vertical density $\overline{V}$ has been derived from eq. (8) using R_{LP}.

Results and discussion

There are some merits and demerits of twilight spectroscopy for the study of chemically active trace species. It is assumed that the chemistry of the atmospheric species is not changing during twilight observations. The error in the computation of SCD of absorbing molecules is generally dominated by non-random residual of the fitting. Also, error in slant column occurs due to instrumental noise, uncertainties in cross-sections and interpolation error during the analysis. Inaccuracies in the calculation of AMF come from the hypothesis of constant vertical profile of absorbent gases and aerosols, and their temperature dependence that leads to error in vertical column of these gases[6]. It is possible to obtain real-time measurements of a large number of atmospheric species using a single spectroscope. Twilight spectroscopy is particularly valuable to make a detailed study of the air chemistry, where the simultaneous measurements of a large number of species are required in order to study the coupling between them[25]. Using this technique, the atmospheric species are measured in an air column several kilometres long, which averages out very localized sources of emission giving rise to a more representative picture of the area. Especially hydroxyl (OH) and nitrate (NO_x) radicals, which are important in tropospheric ozone chemistry, can only be measured using this technique. Thus, twilight spectroscopy is an inexpensive technique compared to other methods and can be efficiently used to monitor long-term changes of different atmospheric species.

Ozone is evaluated in the spectral region 462–498 nm where transitions in the Chappuis band occur. In this spectral region, O_3 together with NO_2, H_2O and O_4 is included in the fitting procedure[22]. In addition, the contribution of the rotational Raman scattering on air particles (ring effect) is treated in the evaluation by including pseudo cross-sections as the inverse of the twilight spectrum[17]. In order to check the origin of errors, we have analysed the structure of the residuals (the differences between the calculated and measured in terms of the total differential optical depth (TDOD)) for 462–498 nm region. Figure 5 shows a typical set of fits. The top plot is the overall fit (the differential $-\ln[I/I_0]$) and in the lower panels, the individual concentrations to the observed

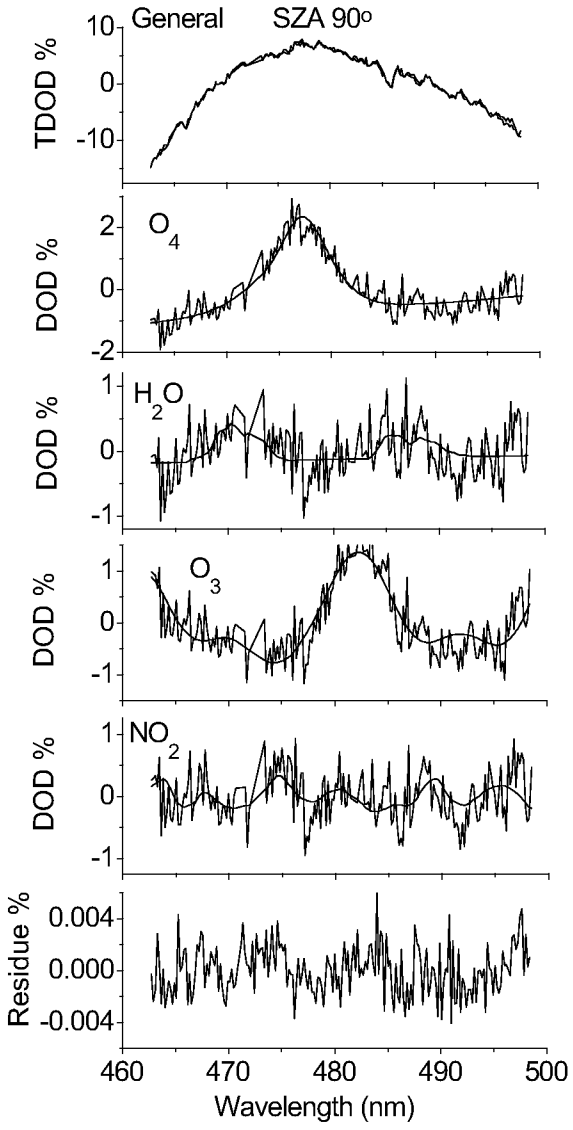

Figure 5. Comparison and contribution of observed and calculated DODs of absorbers O_3, NO_2, H_2O and O_4 to the total absorption. The top plot shows the fit obtained including all parameters in the evaluation (O_3, NO_2, H_2O, O_4, Rayleigh and ring effect).

absorptions are shown. The DODs of O_3, NO_2, H_2O, O_4 and residuals are found to be 1.4, 0.6, 0.5, 2.3 and 0.002%, respectively during morning hours on 12 May 2000 at 90° SZA with reference 38.4° SZA of the same day. We find good agreement between observed and calculated DODs. The resulting residual is low, and arises mainly from incomplete removal of the Fraunhofer structure.

The absolute absorption cross-sections of NO_2 and O_3 at 479 nm, 3.38×10^{-19} mol/cm^2 and 6.78×10^{-22} mol/cm^2, respectively are considered for calculating AMFs. The density profiles of O_3 and NO_2 are assumed as Gaussian profiles, adopted from McClatchey *et al.*[26] and Noxon *et al.*[8], with TCD 6.97×10^{18} mol/cm^2 and 5.77×10^{15} mol/cm^2, respectively and used in radiative transfer model. Figure 6 *a* and *b* shows the NO_2 and O_3 plots of AMF with SZA at 15, 20, 25 and 30 km level. Minimum deviation in Langley plots from fitted straight line is observed at 25 km level. Therefore, the AMFs of 25 km level are considered for calculation of TCDs. Plots of SCDs and TCDs of O_3 with SZA of four days, namely 23, 24, 25 and 26 November 2000 are shown in Figure 7 *a–c* respectively. The SCDs are found to increase with increase in SZA due to increasing path length at higher SZA. All plots of O_3 SCDs with AMFs show a linear trend with a little scatter, as seen in Figure 7 *b*. Little variation is seen in O_3 TCDs after 90° SZA, a variation of 3 to 7 DU which could be due to multiple scattering. The straight line in Figure 7 *c* shows the Dobson spectrophotometer value. Vertical column density of ozone obtained by other methods is given in Table 1. The agreement is good. The slopes of Langley plots (V_{LP}) give the underestimated values with respect to the Dobson total ozone (V_{Dob}). The slant amount of ozone in the reference spectrum is calculated from the intercept of Langley plots. The average TCDs $\overline{V}$ and V_{90} are derived using R_{LP} and they are in good agreement with Dobson spectrophotometer observations which are collected from World Ozone Data Center (WODC), Pune station.

Daily TCDs of NO_2 and O_3 obtained at Pune (18°32′N, 73°51′E) in the morning and evening twilight hours during the period 4 May 2000 to 31 May 2001 are shown in Figure 8 *a* and *b*, respectively. These data were derived from SCDs at 90° SZA using the AMF, calculated by radiative transfer model. Data were not available from day number 404 to 451, therefore they have been shown by straight line in the figure. Earlier spectroscopic studies at Pune showed that the TCDs of NO_2 and O_3 varied from 1.3×10^{16} to 0.6×10^{16} mol/cm^2 and 285 to 239 DU, respectively from May 1988 to February 1989 (ref. 5). Presently, 1.4×10^{15} mol/cm^2 (morning average) and 2.8×10^{15} mol/cm^2 (evening average) of NO_2 in the vertical column are observed during December 2000–January 2001 (winter). In May 2001 (summer), average TCD of NO_2 is 4.6×10^{15} mol/cm^2 and 7.8×10^{15}mol/cm^2 observed in the morning and evening twilight hours, respectively at Pune. Similarly, average morning TCD of NO_2 is 4.9×10^{15} mol/cm^2 and average evening value is 7.9×10^{15} mol/cm^2 during May 2000. Average morning and evening TCDs of NO_2 is 2.1×10^{15} mol/cm^2 in December 2000–January 2001, 6.2×10^{15} mol/cm^2 in May 2001 and 6.4×10^{15} mol/cm^2 in May 2000. The ratio of summer to winter densities of NO_2 is 2.95 and for O_3 it is 1.21. Lal *et al.*[27] have made some NO_2 measurements at Ahmedabad (23°N, 72°E) in the spectral range 436–448 nm. TCDs of NO_2 were noticed between 0.5 and 2.5×10^{15} mol/cm^2 (average 1.5×10^{15}) during December 1989–January 1990 (winter), which are lower than the present winter value 2.1×10^{15} mol/cm^2 at Pune. The ratio of NO_2 (PM/AM) was found to be 1.25, maximum in December; then it had a decreasing trend at Ahmedabad. At Pune, the ratio is 2.0 in December and decreased up to 1.7 in May 2001. Thus the similar trend in ratio is observed at Pune.

During daytime, photochemical reactions take place in the presence of sunlight and N_2O_5 that formed due to oxidation of NO_2 during night gets photolysed to reproduce NO_2. The formation of NO_2 during the day leads to

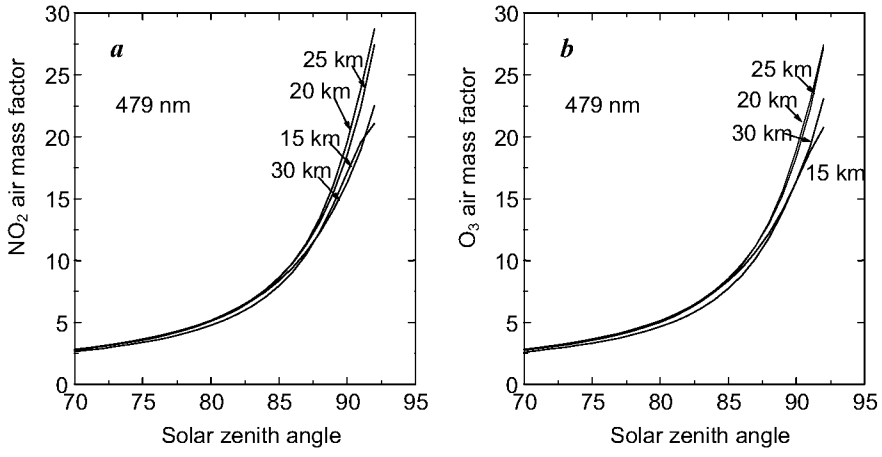

Figure 6. AMF of NO_2 and O_3 with SZA assuming various layer heights.

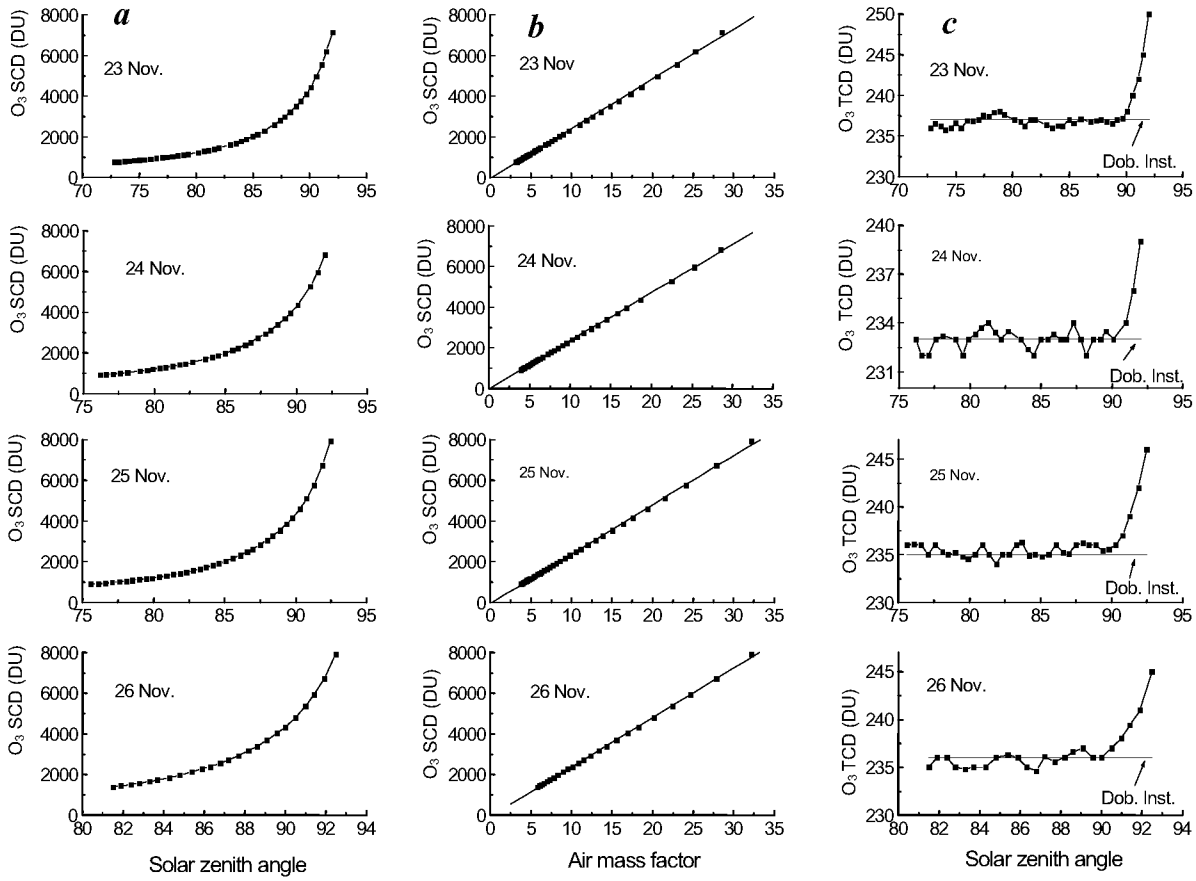

Figure 7. Measurement of ozone density in November 2000. *a*, Ozone SCD with SZA; *b*, Ozone SCD with AMF; *c*, Comparison of TCD of ozone with Dobson spectrophotometer values.

Table 1. Vertical and slant column densities of ozone in the month of September 2000 using different procedures

Date (2000)	Slope of Langley plot V_{LP} 75 to 92°	$\overline{V}$ 75 to 90°	V_{90}	V_{Dob}	R_{LP}	R_{Dob} = V_{Dob} × AMF
23 September	244	239	238	237	783	760
24 September	236	234	233	233	920	909
25 September	242	236	236	235	907	881
26 September	243	236	236	236	1423	1382

V_{LP} and $\overline{V}$ are calculated using Langley plot and eq. (8), respectively. V_{90} is calculated at 90° SZA using R_{LP}, and V_{Dob} is from Dobson spectrophotometer observations.

increase in the TCDs of NO_2. The increase in NO_2 TCDs is also possible due to increased pollution during day, which is reflected in the evening twilight hours. At twilight, NO_2 density depends on NO and is controlled by the following reactions.

$$NO + O_3 = NO_2 + O_2,$$

$$NO_2 + h\nu = NO + O,$$

$$NO_2 + O = NO + O_2.$$

During the evening twilight hours, the rapid decrease in the rate of photolysis of NO_2 and the abundance of atomic oxygen leads to conversion of NO into NO_2. Thus the total number of NO_2 molecules can increase substantially during evening hours, and hence the AM/PM difference[15,28,29]. This AM/PM difference in TCDs of NO_2 is seen in from Figure 8 *a*. However, there is not much difference seen in O_3 values (Figure 8 *b*).

In summer, the length of the day increases due to movement of the sun and hence the duration of sunlight hours leads to further photolysis of N_2O_5 which causes higher TCDs of NO_2 as compared to winter values[13]. The TCD data at Pune show strong seasonal and diurnal variations of NO_2, with maxima in summer at sunset and minima in winter at sunrise. This agrees with the results

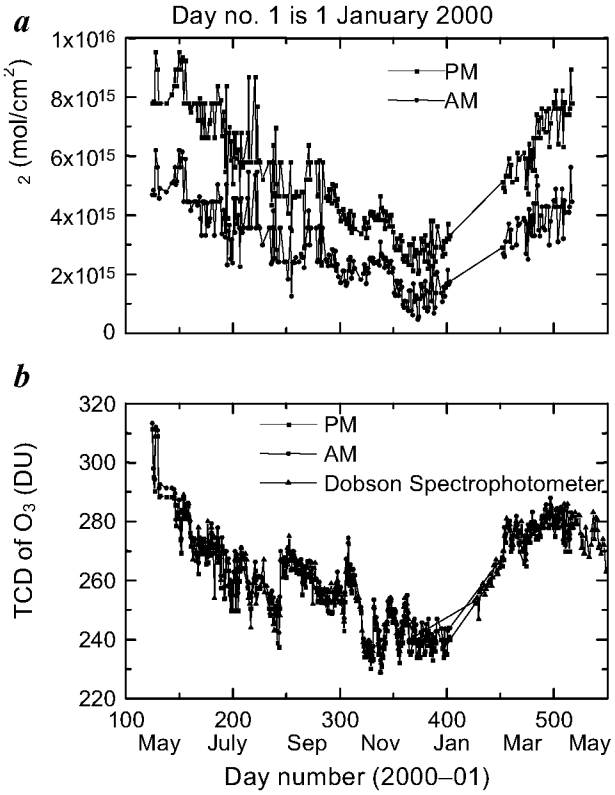

Figure 8. Time series of total column density of NO_2 and O_3 at sunrise (AM) and sunset (PM), at Pune (18°32′N, 73°51′E) during May 2000–May 2001.

of earlier workers[5,8–13,27]. Also, more ozone is confined to increased duration of UV-radiation during summer months. Ozone produced in the tropical region gets transported to higher latitudes by the stratospheric mean diabatic circulation. Ozone-rich air during winter moves poleward and downward, which explains the seasonal variation in ozone. Also, day-to-day variability in total ozone is caused by changing weather patterns in the troposphere and its effects may extend to the lower stratospheric levels. Ozone has strong seasonal variation but weak diurnal variation, with maxima in the summer and minima in the winter.

Conclusions

A single scattering radiative transfer model has been developed to calculate the AMFs for scattered light observations. These AMFs are used for determining the TCDs of NO_2 and O_3. Various methods of evaluating TCD are discussed. The mean difference of our preferred method for calculating vertical ozone from the spectrometer was 3 DU. Possible changes in ozone during the course of the day lead us to recommend the range 75–90° SZA for determination of both slope and intercept of Langely plots. The average TCDs $\overline{V}$ and V_{90} derived using R_{LP} are in good agreement with the Dobson spectrophotometer observations. A good matching is achieved between observed and calculated DODs of NO_2, O_3, H_2O and O_4. It is observed that evening NO_2 TCDs are higher than those in the morning. It is also found that the TCDs of O_3 in the morning are higher than those in the evening.

A time series of daily TCDs of NO_2 and O_3 is obtained from observations made at Pune, (18°32′N, 73°51′E) using automatic visible spectrometer during May 2000–May 2001. This study reveals large day-to-day variability in TCDs of NO_2 than in O_3, with maxima in summer and minima in winter.

1. Brewer, A. W., McElroy, C. T. and Kerr, J. B., Nitrogen dioxide concentrations in the atmosphere. *Nature*, 1973, **246**, 129–133.
2. Noxon, J. F., Nitrogen dioxide in the stratosphere and troposphere measured by ground based spectroscopy. *Science*, 1975, **189**, 547–549.
3. Platt, U. and Permer, D., Measurement of atmospheric trace gases by long path differential UV visible absorption spectroscopy. *Springer Ser. Opt. Sci.*, 1983, **39**, 95–105.
4. Pommereau, J. P. and Goutail, F., Ground based measurements by visible spectroscopy during the Arctic winter and spring. *Geophys. Res. Lett.*, 1988, **15**, 891–894.
5. Bhonde, S. D., Mehra, P., Bose, S., Londhe, A. L. and Jadhav, D. B., Simultaneous measurements of low latitude NO_2 and O_2 from zenith sky observations in visible region. *Indian J. Radio Space Phys.*, 1992, **21**, 18–25.
6. Gil, M., Puentedura, O., Yela, M., Parrondo, C., Jadhav, D. B. and Thorkelsson, B., OClO, NO_2 and O_3 total column observations over Iceland during the winder 1993–94. *Geophys. Res. Lett.*, 1996, **23**, 3337–3340.
7. Solomon, S., Portmann, R. W., Sanders, R. W., Daniel, J. S., Madson, W., Bartram, B. and Dutton, E. G., On the role of nitrogen dioxide in the absorption of solar radiation. *J. Geophys. Res.*, 1999, **104**, 12047–12058.
8. Noxon, J. F., Whipple, E. C. and Hyde, R. S., Stratospheric NO_2, observational method and behavior at mid latitude. *J. Geophys. Res.*, 1979, **84**, 5047–5065.
9. Syed, M. Q. and Harrison, A. W., Seasonal trend of stratospheric NO_2 over Calgary. *Can. J. Phys.*, 1981, **59**, 1278–1279.
10. Johnston, P. V. and Mckenzie, R. L., NO_2 observations at 45°S during the decreasing phase of solar cycle 21, from 1980 to 1987. *J. Geophys. Res.*, 1989, **94**, 3473–3486.
11. Solomon, S. and Keys, J. G., Seasonal variations in Antarctic NO_x chemistry. *J. Geophys. Res.*, 1992, **97**, 7971–7978.
12. Kondo, Y. *et al.*, Ground based measurements of column amounts of NO_2 over Syowa station, Antarctica. *J. Geophys. Res.*, 1994, **99**, 14535–14548.
13. Nichol, S. E., Keys, J. G., Wood, S. W., Johnston, P. V. and Bodeker, G. E., Intercomparison of total ozone data from a Dobson spectrometer, TOMS, visible wavelength spectrometer, and ozonesondes. *Geophys. Res. Lett.*, 1996, **23**, 1087–1090.
14. Noxon, J. F., Norton, R. B. and Henderson, W. R., Observation of atmospheric NO_3. *Geophys. Res. Lett.*, 1978, **5**, 675–678.
15. Solomon, S., Schmeltekopf, A. Z. and Sanders, R. W., On the interpretation of zenith sky absorption measurement. *J. Geophys. Res.*, 1987, **D92**, 8311–8319.
16. Wagner, T. *et al.*, Cloudy sky optical paths as derived from DOAS observations. *J. Geophys. Res.*, 1998, **103**, 25307–25321.
17. Mckenzie, R. L. and Johnston, P. V., Seasonal variations in stratospheric NO_2 at 45°S. *Geophys. Res. Lett.*, 1982, **9**, 1255–1258.

18. *Handbook of Geophysics and Space Environment*, McGraw-Hill, New York, 1965.
19. Jadhav, D. B., Londhe, A. L., Meena, G. S., Dhanjay Jhurry and Rossett, J. M., Installation of an automatic spectrometer at Mauritius and preliminary results of NO_2 over Mauritius. *Curr. Sci.*, 1999, **76**, 998–1000.
20. Meena, G. S., Padma Kumari, B. and Jadhav, D. B., An automatic rotating slit scanning spectrometer for atmospheric studies. Proceedings of the National Workshop on Atmospheric Chemistry (eds Devara, P. C. S. and Raj, P. E.), Pune, 2002, pp. 155–158.
21. Platt, U., Perner, D. and Patz, W., Simultaneous measurements of atmspheric CH_2O, O_3 and NO_2 by differential optical absorption. *J. Geophys. Res.*, 1979, **84**, 6329–6335.
22. Gil, M., Puentedura, O. and Yela, M., Behaviour of NO_2 and O_3 columns during the eclipse of 26 February 1998, as measured by visible spectroscopy. *J. Geophys. Res.*, 2000, **105**, 3583–3593.
23. Pommereau, J. P., Gootail, F., Pinharanda, M., Piquard, J. and Sarkission, A., First European Workshop on Polar Stratospheric Ozone Research (eds Pyle, J. and Harris, N.), Cambridge, 1991, pp. 41–44.
24. Van Roozendael, M., Deinaziere, M. and Simon, P. C., Ground-based visible measurements at the Jungfraujoch station since 1990. *J. Quant. Spectrosc. Radiat. Transfer.*, 1994, **52**, 231–240.
25. Plane, J. M. C. and Nien, C. F., Differential optical absorption spectrometer for measuring atmospheric trace gases. *Rev. Sci. Instrum.*, 1992, **63**, 1867–1876.
26. McClatchey, R. A., Feun, R. W., Selby, J. E. A., Volz, F. E. and Garing, J. S., *Optical Properties of the Atmosphere*, Air Force Cambridge Research Laboratories, Bedford, MA, 1972, 3rd edn.
27. Lal, M., Chakrabarty, D. K., Sidhu, J. S., Das, S. R. and Verma, S. D., Some results of ground-based measurements of atmospheric NO_2 at Ahmedabad by visible absorption spectroscopy. *Indian J. Radio Space Phys.*, 1993, **22**, 108–113.
28. Kerr, J. B., Evans, W. F. J. and McConnell, J. C., The effects of NO_2 changes of twilight on trangent ray NO_2 measurements. *Geophys. Res. Lett.*, 1977, **4**, 577–579.
29. Boughner, R., Larsen, J. C. and Natarajan, M., The influence of NO and ClO variations at twilight on the interpretation of solar occultation measurements. *Geophys. Res. Lett.*, 1980, **7**, 231–234.

ACKNOWLEDGEMENTS. We thank the Head, Physical Meteorology and Aerology Division and the Director of IITM, Pune for their continuous encouragement in carrying out this work. We also thank DST for providing financial support for development of the spectrometer.

Received 13 January 2003; revised accepted 6 May 2003

Orbital forcing of the Plio-Pleistocene Indian monsoons: benthic foraminiferal proxies from ODP Site 758

Anil K. Gupta[†,*] and Jean-Luc Mélice[#]

[†]Department of Geology and Geophysics, Indian Institute of Technology, Kharagpur 721 302, India
[#]Institut de Recherche pour le Développement, Laboratoire d'Océanographie Dynamique et de Climatologie, Université Pierre et Marie Curie, Paris, France

The Indian Ocean monsoon system is one of the dominant features of the earth's climate influencing weather and climate of the Asian region. Long-term changes in the monsoon have been linked to orbital forcings as well as the Himalayan–Tibetan uplift. Changes in the monsoon are preserved in various proxies across the region both on land and in the marine sediments. Here we present Plio-Pleistocene record of monsoon proxy deep-sea benthic foraminifera from Ocean Drilling Programme Site 758, northeast ern Indian Ocean to understand a link between orbital changes and Indian Ocean monsoon variability. We used Continuous Wavelet Transform (CWT) of *Uvigerina proboscidea* and *Epistominella exigua*, which have been found blooming in two different seasons of the Indian monsoon – the summer and winter monsoons, respectively. An inverse relation between the two is observed during the past ~1000 kyr in the CWT-extracted 400-kyr components as also in the raw data. The variable relation between the monsoon proxies and earth's eccentricity at Site 758 agrees with the recent findings that orbital forcing of the Indian monsoon shows major shifts during the Plio-Pleistocene. These shifts correspond to the advent of growth and decay of the Northern Hemisphere ice sheets since the last 2.5 Ma.

THE Indian Ocean climate is dominated by the summer or southwest (SW) monsoon and winter or northeast (NE) monsoon winds, affecting weather and climate of the Asian and African regions between 30°N and 20°S latitudes[1]. Winds are stronger and precipitation is high during the summer monsoon season, whereas during the winter monsoon months weak and variable winds cause low precipitation. Both sensible and latent heating drive the summer monsoon winds between the cold Indian Ocean and the warmer Indian–Asian land mass (Himalayan–Tibetan Plateau) during May–July[2]. During winter,

*For correspondence. (e-mail: anilg@gg.iitkgp.ernet.in)